Supporting information for

Surface-Dependent Stability of the Interface between Garnet $Li_7La_3Zr_2O_{12}$ and the Li Metal in the All-Solid-State Battery from First-Principles Calculations

Bo Gao[a], Randy Jalem[a,b,c,d], Yoshitaka Tateyama[a,b,c,*]

[a]*Center for Materials Research by Information Integration (CMI²), Research and Services Division of Materials Data and Integrated System, National Institute for Materials Science (NIMS), 1-1 Namiki, Tsukuba, Ibaraki 305-0044, Japan*

[b]*Center for Green Research on Energy and Environmental Materials (GREEN), Global Research Center for Environment and Energy based on Nanomaterials Science, and International Center for Materials Nanoarchitectonics (MANA), NIMS, 1-1 Namiki, Tsukuba, Ibaraki 305-0044, Japan*

[c]*Elements Strategy Initiative for Catalysts & Batteries, Kyoto University, 1-30 Goryo-Ohara, Nishikyo-ku, Kyoto 615-8245, Japan*

[d]*PRESTO, Japan Science and Technology Agency (JST), 4-1-8 Honcho, Kawaguchi, Saitama 333-0012, Japan*

*TATEYAMA.Yoshitaka@nims.go.jp

Section 1. Structure parameters of the tetragonal and cubic LLZO bulk phases

Table S1 Calculated lattice parameters of t-LLZO and c-LLZO bulk phases

		a (Å)	b (Å)	c (Å)
t-LLZO	Our work	13.205	13.205	12.675
	Experiment[1]	13.134	13.134	12.663
c-LLZO	Our work	13.03	13.03	13.03
	Experiment[2]	13.00	13.00	13.00

Section 2. Construction of LLZO/Li interface

Here the low-index surfaces of LLZO are adopted, including (100), (001), (101) and (110) facets, to construct the interface with Li metal. Firstly, the coincident superlattice for LLZO and Li metal is needed to be identified to avoid the large internal stress induced by the lattice mismatch, which decrease the interface stability. The 4×4 supercell of (100) surface of bcc-type Li crystal is used to match the (100) and (001) surfaces of LLZO, and the 4×4 supercell of (110) surface of Li crystal is used to match the (110) and (101) surfaces of LLZO. The lattice mismatch values have been calculated using the lattice matching module in CALYPSO software[3], and shown in Table S2. The small mismatch values indicate that the superlattices between LLZO and Li is considerably matched, thus we can use them to construct the interface models.

Table S2 The lattice-matched superlattices for LLZO and Li metal. u and v represent the lengths of vectors of created superlattice. γ is the angle between two surface vectors. $\bar{\boldsymbol{\varepsilon}}$ refers to the average value of lattice-mismatch strain[3].

	u (Å)	v (Å)	γ	$\bar{\boldsymbol{\varepsilon}}$ (%)
LLZO(100)	13.205	12.675	90	2.868
4×4 Li(100)	13.728	13.728	90	
LLZO(001)	13.205	13.205	90	1.903

4×4 Li(100)	13.728	13.728	90	
LLZO(101)	11.285	11.285	71.617	2.835
4×4 Li(110)	11.889	11.889	70.529	
LLZO(110)	11.285	11.285	68.332	3.781
4×4 Li(110)	11.889	11.889	70.529	

The simulated model for LLZO/Li interface can be built based on the searched coincident superlattice, as shown in Fig. S1(a). In a unit cell, there are two equivalent interfaces which can effectively prevent the dipole effect induced by the interfacial polarization. In order to sufficiently cover the search space in the search of the energetically stable configuration, the rigid-body displacement between LLZO and Li [illustrated in Fig.S1(a)] have been involved. Especially for lateral displacements ($\mathbf{d_u}$ and $\mathbf{d_v}$), a 4×4 grid which includes 16 different structures is adopted. The test [Fig. S1(b)] shows that the use of this grid can effectively cover on the energetically favorable and unfavorable region. For the vertical displacement ($\mathbf{d_w}$), two tests have been performed on the different interfaces. Both test results [Fig.S1(c) and (d)] show that interface structure with initial vertical displacement of 2 Å is energetically stable. Therefore, the initial vertical displacement is set to 2 Å the search of stable interface structure.

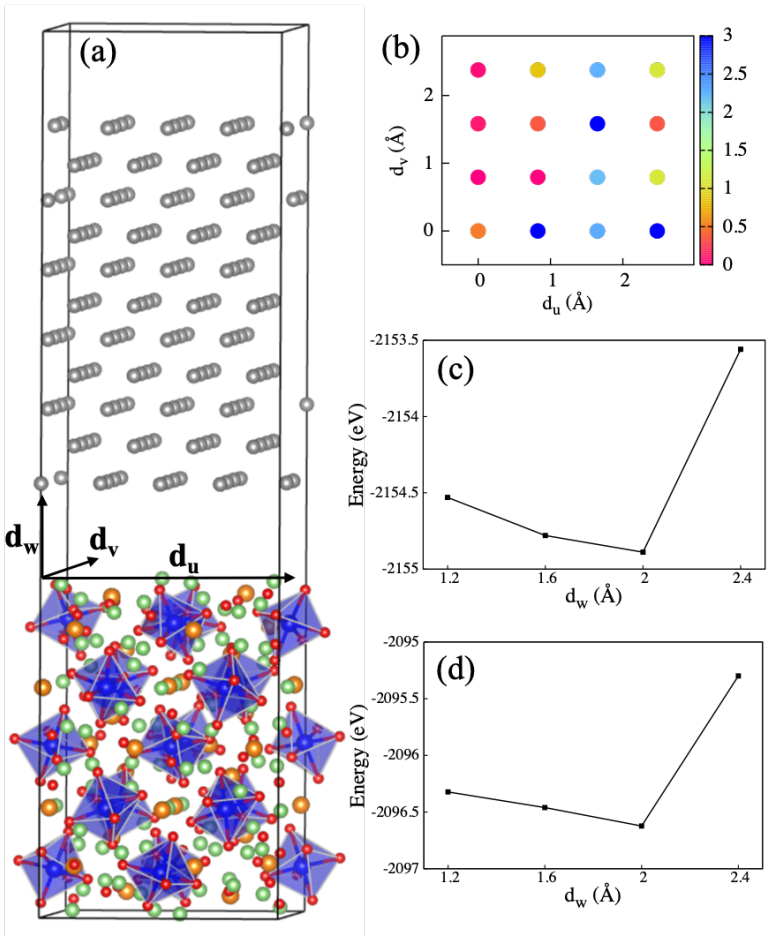

Figure S1. (a) Schematic structure model adopted in our simulation of LLZO/Li interface. The grey, green, orange, blue and red spheres represent Li in Li metal, Li in LLZO, La, Zr and O atoms, respectively. (b) The calculated energy distributions as a function of rigid-body displacement along lateral directions in LLZO(100)/Li(100) interface. The color bar represents the energy deviation with respect to the stable configuration. (c), (d) The energetic variation as a function of rigid-body displacement along vertical direction in two LLZO(100)/Li(100) interfaces.

Table S3 Selected chemical potentials (eV) of Li, La, Zr and O in LLZO under reducing environment. The Li metal, La_2O_3 and Zr metal phases are taken as the reference phases. The similar reducing conditions have been used in previous calculations.[4,5]

	$\Delta\mu_{Li}$	$\Delta\mu_{La}$	$\Delta\mu_{Zr}$	$\Delta\mu_{O}$
Reducing	0	-0.408	0	-6.21

Table S4 Surface energies (γ_{surf}) under reducing environment calculated in current and previous works of reported LLZO surface terminations.

	γ_{surf} (J/m^2)
(100) Li-terminated	0.872
	0.87±0.02 [Ref. 4]
(001) Li-terminated	1.084
	1.08 [Ref. 5]
(110) La,Li-terminated	1.067
	1.04 [Ref. 5]

Table S5 Considered surface compositions in the search of energetically stable surface terminations of LLZO.

(100)	(001)	(101)	(110)
Stoichiometric	Stoichiometric	Stoichiometric	Stoichiometric
Li_5LaO_4	Li_3LaO_3	Li_2O	Li_2O
$LiLaO_2$	Li_5LaO_4	Li_3LaO_3	$LiLaO_2$
Li_3LaO_3	Li_7LaO_5	$Li_4La_2O_5$	Li_3LaO_3
$Li_2La_2Zr_2O_8$	$La_2Zr_2O_7$	$Li_5La_3O_7$	$Li_2Zr_2O_5$
$Li_6La_4Zr_2O_{13}$	$Li_2La_2Zr_2O_8$	$Li_4La_2Zr_2O_9$	$Li_4La_2O_5$
	$Li_4La_2Zr_2O_9$	$Li_6La_2Zr_2O_{10}$	$Li_5La_3O_7$
	$Li_4La_4Zr_2O_{12}$		$Li_4La_2Zr_2O_9$
	$Li_{10}La_2Zr_2O_{12}$		$Li_6La_4Zr_2O_{13}$

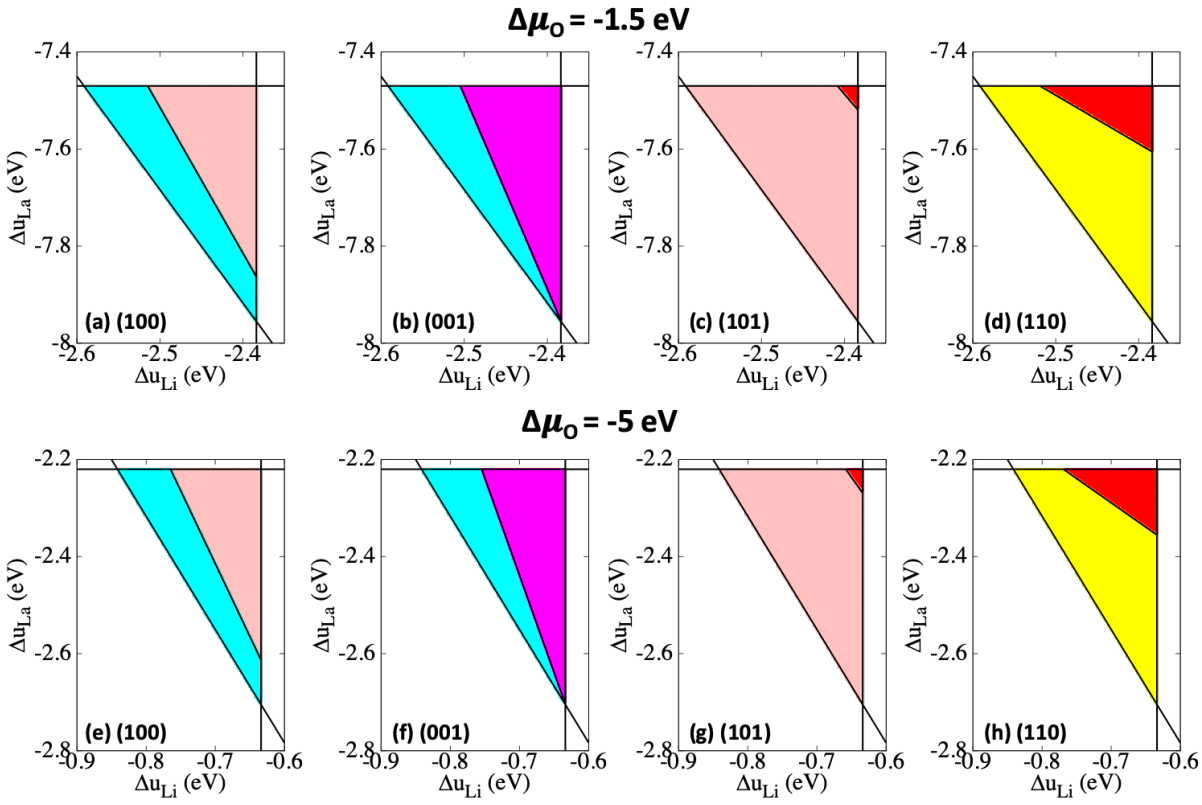

Figure S2. Calculated phase diagrams of (100) (a, e), (001) (b, f), (101) (c, g) and (110) (d, h) surfaces of LLZO under selected O-rich ($\Delta\mu_O$= -1.5 eV) and O-poor ($\Delta\mu_O$= -5 eV) chemical potentials. $\Delta\mu_{Li}$ and $\Delta\mu_{La}$ represent the chemical potentials with respect to the Li and La metals, respectively. The color of each stable termination represents the proportion of 5-coordinated Zr on the surface. The cyan, yellow, pink, magenta and red represent 100%, 75%, 50%, 25%, 0% of 5-coordinated Zr on the surface termination, respectively.

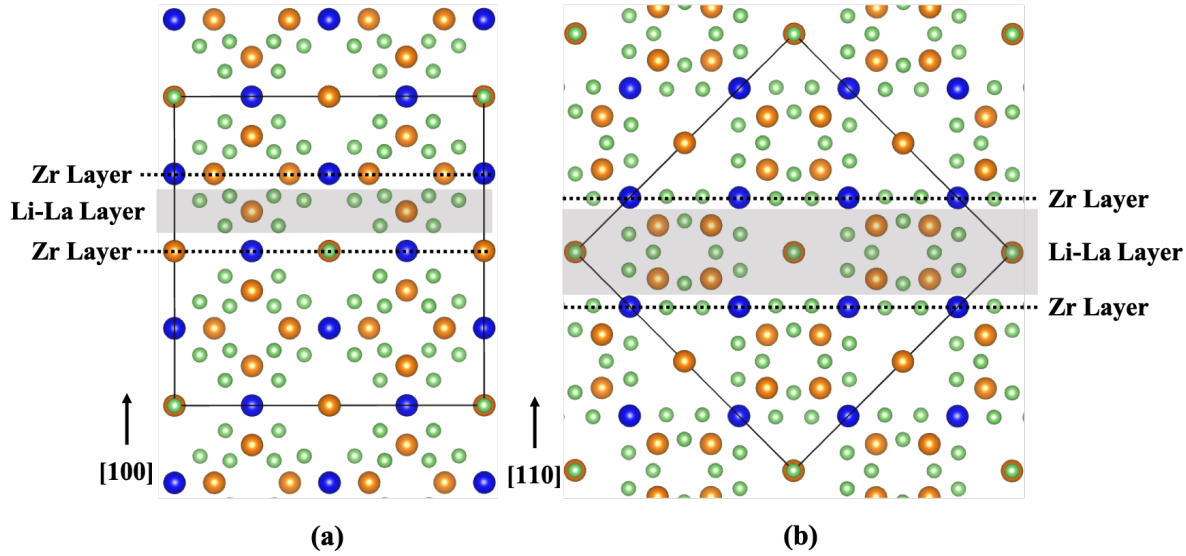

Figure S3. The distributions of Zr and Li, La layer along [100] (a) and [110] (b) directions in LLZO bulk structure. The green, orange and blue balls represent the Li, La and Zr atoms, respectively. The O atoms are not shown in the figure.

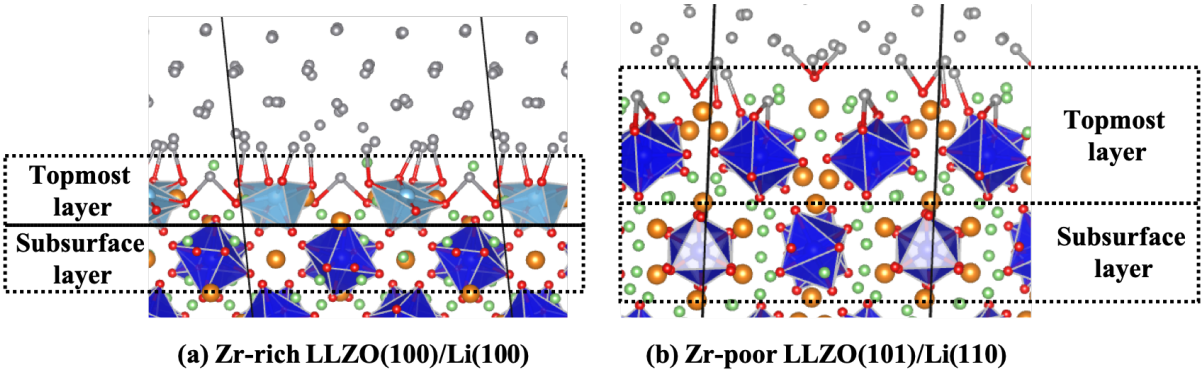

Figure S4. The illustrations of topmost and subsurface layers of LLZO for Zr-rich LLZO(100)/Li(100) (a) and Zr-poor LLZO(101)/Li(110) (b) interfaces used in the layer-decomposed DOS calculation. The green, orange, red, spheres represent Li, La, O atoms, respectively. The light blue and dark blue spheres indicate the Zr_{5c} and Zr_{6c} atoms, respectively. The light and dark blue polyhedrons refer to the ZrO_5 and ZrO_6 units, respectively. Note that in Zr-rich LLZO(100)/Li(100) interface, the subsurface layer contains the O atoms in the topmost ZrO_5 layer.

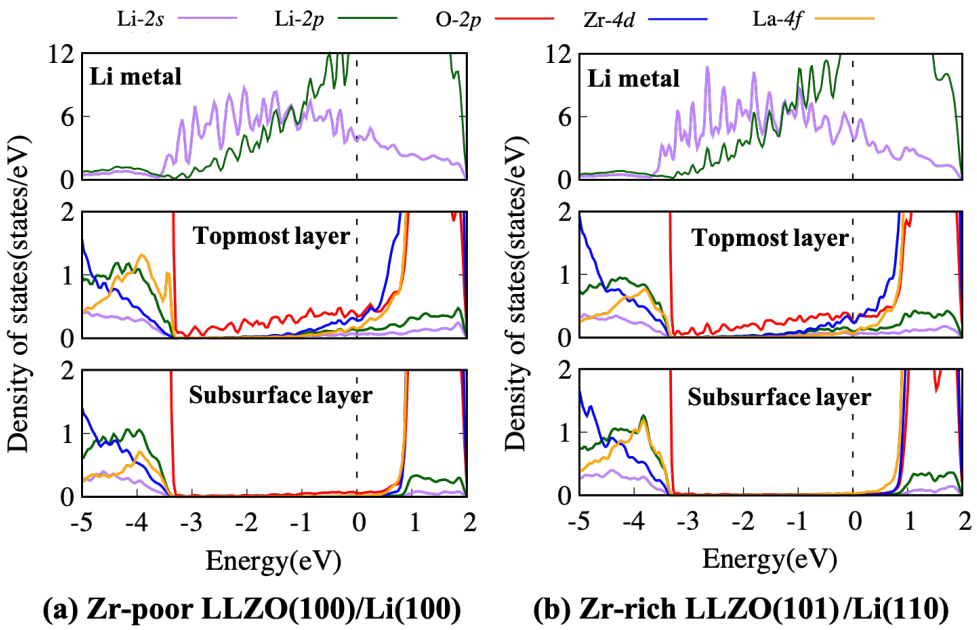

Figure S5. Calculated layer-decomposed PDOSs of the interfaces of Zr-poor LLZO(100)/Li(100) (a) and Zr-rich LLZO(101)/Li(110) (b). The dashed line indicates the Fermi level. The topmost and subsurface layers represent the layers centralized in the topmost and subsurface Zr, respectively.

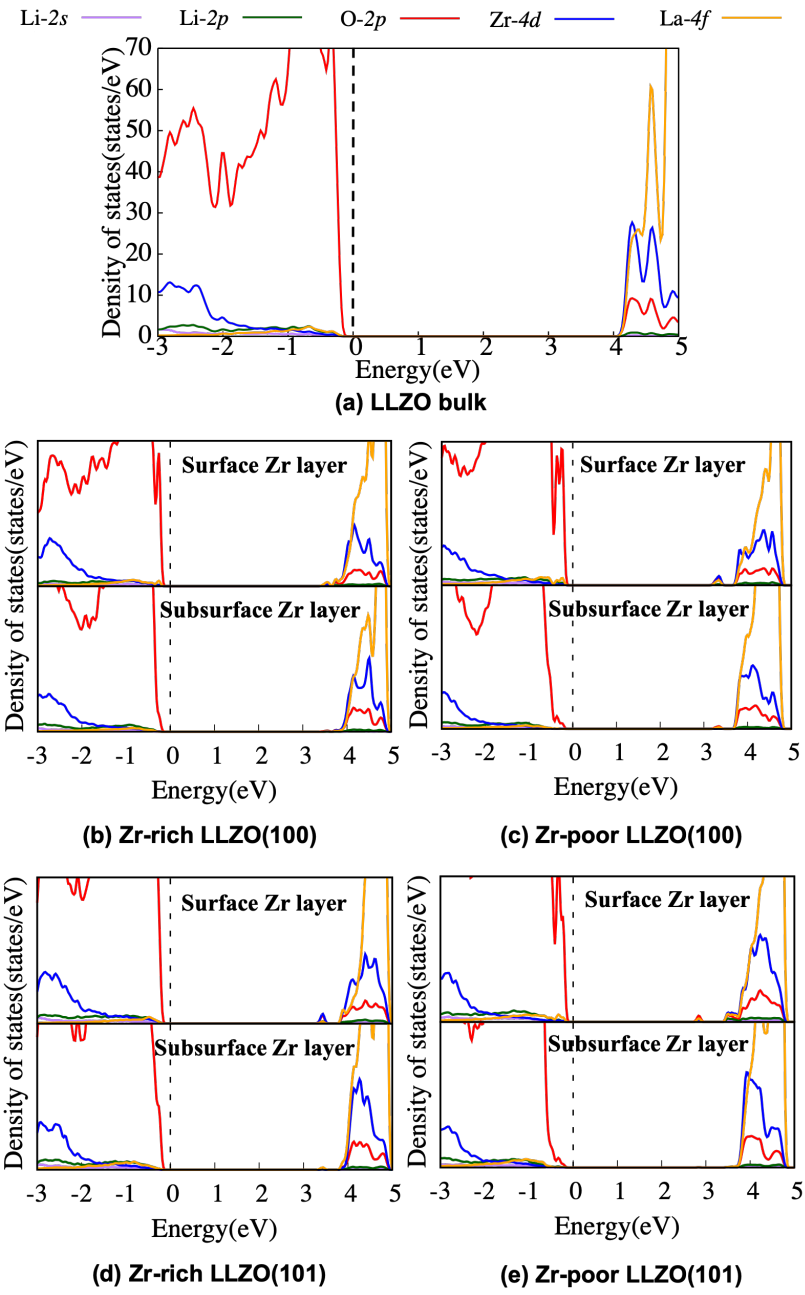

Figure S6. Calculated PDOSs of LLZO bulk (a), and layer-decomposed PDOSs of Zr-poor and Zr-rich (100) and (101) surfaces (b – e). The dashed line in each figure indicates the Fermi level. In (b) – (e), the surface and subsurface Zr layers represent the layers centralized in the surface and subsurface Zr sites, respectively.

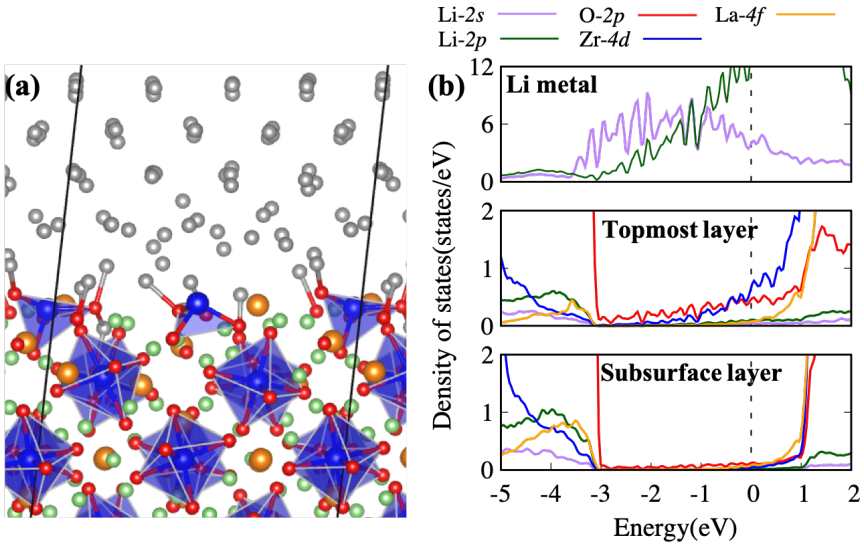

Figure S7. (a) The metastable interface structure composed of LLZO(001)-(Zr termination) and Li(100) surfaces. The color scheme for the atoms and polyhedrons are same with Fig.S4. Notably, there are ZrO_3 and ZrO_4 units at interface. (b) The calculated layer-decomposed PDOS of LLZO(001)-(Zr termination)/Li(100) interface. The topmost and subsurface layers represent the layers centralized in the topmost and subsurface Zr, respectively.

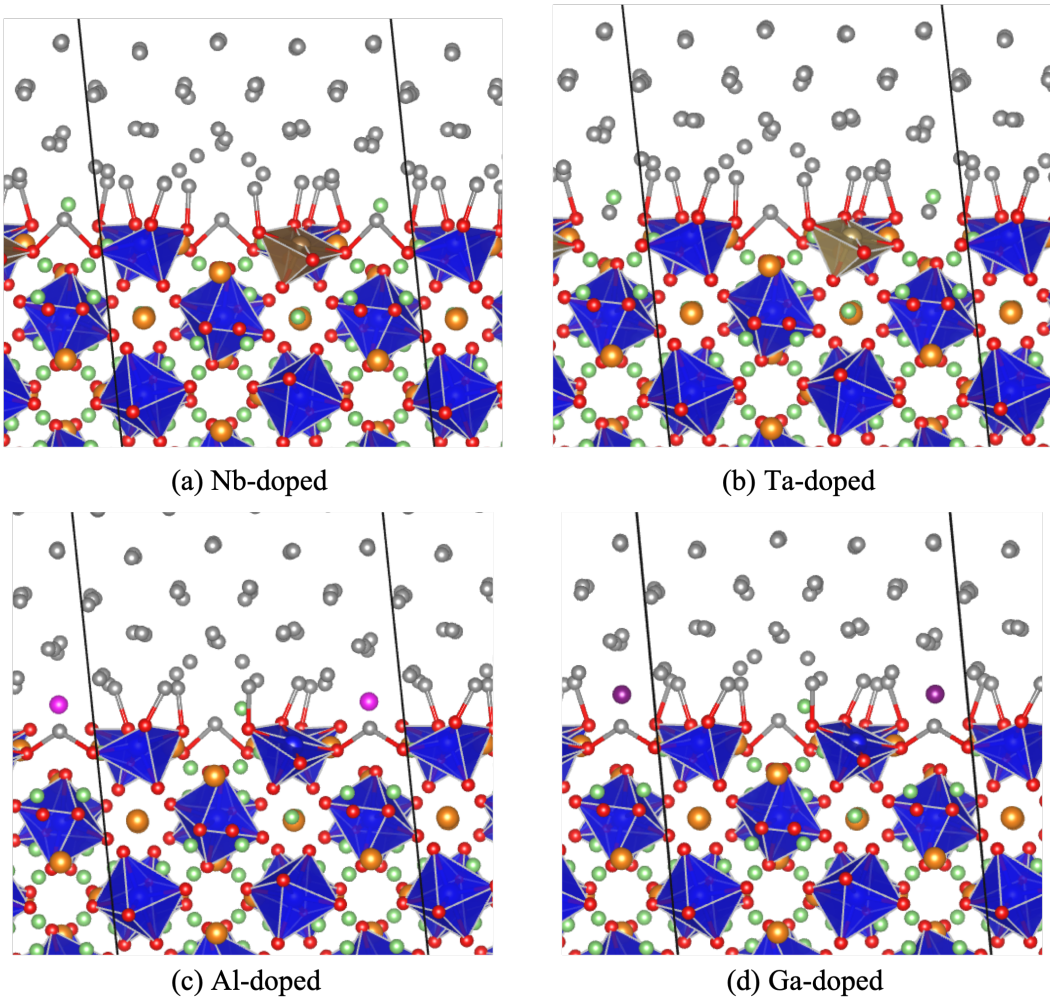

Figure S8. The structures of Zr-rich LLZO(100)/Li(100) interface doped with Nb (a), Ta (b), Al (c) and Ga (d). The color scheme for Li, La, Zr and O atoms are same with Fig.S4. The dark and light brown, magenta and purple spheres represent the Nb, Ta, Al and Ga dopants, respectively.

References

(1) Awaka, J.; Kijima, N.; Hayakawa, H.; Akimoto, J. Synthesis and Structure Analysis of Tetragonal $Li_7La_3Zr_2O_{12}$ with the Garnet-Related Type Structure. *Journal of Solid State Chemistry* **2009**, *182*, 2046–2052. https://doi.org/10.1016/j.jssc.2009.05.020.

(2) Xie, H.; Alonso, J. A.; Li, Y.; Fernández-Díaz, M. T.; Goodenough, J. B. Lithium Distribution in Aluminum-Free Cubic Li7La3Zr2O12. *Chem. Mater.* **2011**, *23* (16), 3587–3589. https://doi.org/10.1021/cm201671k.

(3) Gao, B.; Gao, P.; Lu, S.; Lv, J.; Wang, Y.; Ma, Y. Interface Structure Prediction via CALYPSO Method. *Science Bulletin* **2019**, *64*, 301–309. https://doi.org/10.1016/j.scib.2019.02.009.

(4) Canepa, P.; Dawson, J. A.; Sai Gautam, G.; Statham, J. M.; Parker, S. C.; Islam, M. S. Particle Morphology and Lithium Segregation to Surfaces of the $Li_7La_3Zr_2O_{12}$ Solid Electrolyte. *Chem. Mater.* **2018**, *30*, 3019–3027. https://doi.org/10.1021/acs.chemmater.8b00649.

(5) Tian, H.-K.; Xu, B.; Qi, Y. Computational Study of Lithium Nucleation Tendency in $Li_7La_3Zr_2O_{12}$ (LLZO) and Rational Design of Interlayer Materials to Prevent Lithium Dendrites. *Journal of Power Sources* **2018**, *392*, 79–86. https://doi.org/10.1016/j.jpowsour.2018.04.098.